Nuclear Physics B131 (1977) 399-420

PARTIAL-WAVE ANALYSIS OF $K^-p \to \pi^0\Lambda(1520)$ BETWEEN 1710 AND 2170 MeV C.M. ENERGY INCLUDING NEW DATA BETWEEN 1775 AND 1960 MeV

Rutherford Laboratory – Imperial College Collaboration

W. CAMERON, B. FRANEK, G.P. GOPAL, G.E. KALMUS, A.C. McPHERSON, R.T. ROSS * and D.H. SAXON
Rutherford Laboratory

T.C. BACON, I. BUTTERWORTH, R.W.M. HUGHES, P. NEWHAM and R.A. STERN
Imperial College, London

Received 21 July 1977
(Revised 6 September 1977)

We present extracted data for the pure $I = 1$ $\pi^0\Lambda(1520)$ channel from the reaction $K^-p \to K^-p\pi^0$ at 11 incident momenta between 0.96 and 1.355 GeV/c (1775 to 1960 MeV c.m. energy). A partial-wave analysis of this channel has been carried out over a broad c.m. energy range from 1710 to 2170 MeV using data at 27 momenta from this and earlier experiments. The $\frac{5}{2}^-$ $\Sigma(1775)$ and $\frac{7}{2}^+$ $\Sigma(2030)$ resonances are found to decay strongly to this channel. Amplitudes are also obtained for less dominant and less well-established resonances.

1. Introduction

The reaction:

$$K^-p \to K^-p\pi^0 \tag{1}$$

has been investigated at 11 incident momenta between 0.96 and 1.355 GeV/c as described in sect. 2. The quasi two-body process:

$$K^-p \to \pi\Lambda(1520) \tag{2}$$

makes a strong contribution to reaction (1) and data for this channel have been

* Present address: University of Michigan, Physics Department, Ann Arbor, Michigan 48104, USA.

extracted using a 4-variable maximum likelihood fitting technique as described in sect. 3.

These new data have then been combined with previously published data, namely those of the:

(a) Chicago-Heidelberg (CH) Collaboration [1], covering the incident momentum range 0.822 to 1.226 GeV/c;

(b) College de France-Rutherford Laboratory-Saclay-Strasbourg (CRSS) Collaboration [2], over the range 1.263 to 1.843 GeV/c;

(c) CERN-Heidelberg-Munich (CHM) Collaboration [3], over the range 1.42 to 1.80 GeV/c.

Thus data on reaction (2) are available at 27 incident momenta between 0.822 and 1.843 GeV/c and a partial-wave analysis has been carried out over this range ($1710 < E^* < 2170$ MeV) as described in sect. 4. The conclusions drawn from this analysis are given in sect. 5.

2. The data

The new data for reaction (1) come from an exposure of the CERN 2m HBC to a K^- beam at 11 equally spaced incident momenta between 0.96 and 1.355 GeV/c. Details of the exposure, scanning and measuring, beam calibration and cross-section normalization are given in an earlier publication [4].

Kinematic ambiguities between this channel and the elastic channel were resolved in favour of the latter and ambiguities with the $K^-\pi^+n$ and $\bar{K}^0\pi^-p$ channels were resolved on the basis of ionisation measurements. A total of 16 162 events remained after all ambiguities had been resolved. The values of the cross section for reaction (1) obtained after correcting for scanning and through-put losses are given in table 1 and shown in fig. 1. The values are in good agreement with the results of earlier experiments [1,2].

Dalitz plots, together with their projections, are shown in fig. 2 for the lowest, central and highest incident momenta. This 3-body final state has strong contributions from reaction (2) and also the quasi two-body reactions

$$\begin{aligned} K^-p &\to pK^{*-}(890) \\ &\quad\hookrightarrow K^-\pi^0 , \end{aligned} \tag{3}$$

$$\begin{aligned} K^-p &\to K^-\Delta^+(1233) \\ &\quad\hookrightarrow p\pi^0 . \end{aligned} \tag{4}$$

The Kp mass-squared distribution in the region of the $\Lambda(1520)$ ($2.15 \leqslant M^2(Kp) \leqslant 2.46$ GeV^2) obtained by summing data from all eleven momenta is shown in fig.3. The mass and the width of the resonance have been determined by fitting a Breit-Wigner shape [5] with an energy-independent width superimposed on a linear back-

Table 1
Values of cross sections for the $K^-p\pi^0$ final state and for processes contributing to it, at each of the 11 incident momenta

Beam momentum in GeV/c	C.m. energy in GeV	$\sigma[\pi^0\Lambda(1520)]$ mb	$\sigma[K^{*-}(890)P]$ mb	$\sigma[K^-\Delta^*(1233)]$ mb	$\sigma[\pi^0\Lambda(1690)]$ mb	$\sigma[\pi^0\Sigma^0(1775)]$ mb	$\sigma[\pi^0K^-P(\text{LIPS})]$ mb	$\sigma[K^-P\mapsto K^-P\pi^0]$ mb
0.960	1.775	0.656 ± 0.038	0.054 ± 0.007	0.140 ± 0.012			0.083 ± 0.014	0.933 ± 0.049
1.005	1.796	0.550 ± 0.036	0.087 ± 0.010	0.230 ± 0.019			0.098 ± 0.017	0.965 ± 0.052
1.045	1.815	0.417 ± 0.024	0.154 ± 0.012	0.255 ± 0.016			0.282 ± 0.017	1.107 ± 0.047
1.085	1.833	0.298 ± 0.021	0.273 ± 0.019	0.339 ± 0.021			0.169 ± 0.020	1.078 ± 0.048
1.125	1.852	0.287 ± 0.020	0.506 ± 0.027	0.406 ± 0.023	0.049 ± 0.010		0.056 ± 0.011	1.304 ± 0.051
1.165	1.870	0.224 ± 0.015	0.585 ± 0.027	0.386 ± 0.020	0.044 ± 0.018		0.063 ± 0.019	1.301 ± 0.047
1.205	1.889	0.180 ± 0.013	0.650 ± 0.028	0.292 ± 0.016	0.109 ± 0.014		0.071 ± 0.011	1.302 ± 0.047
1.245	1.907	0.160 ± 0.011	0.627 ± 0.024	0.315 ± 0.014	0.089 ± 0.019		0.097 ± 0.011	1.288 ± 0.041
1.285	1.926	0.209 ± 0.013	0.625 ± 0.024	0.345 ± 0.015	0.040 ± 0.005	0.096 ± 0.011	0.019 ± 0.006	1.334 ± 0.041
1.320	1.941	0.178 ± 0.013	0.547 ± 0.023	0.256 ± 0.012	0.043 ± 0.005	0.145 ± 0.015	0.017 ± 0.006	1.185 ± 0.040
1.355	1.957	0.212 ± 0.012	0.629 ± 0.021	0.302 ± 0.012	0.045 ± 0.005	0.184 ± 0.015	0.041 ± 0.010	1.413 ± 0.039

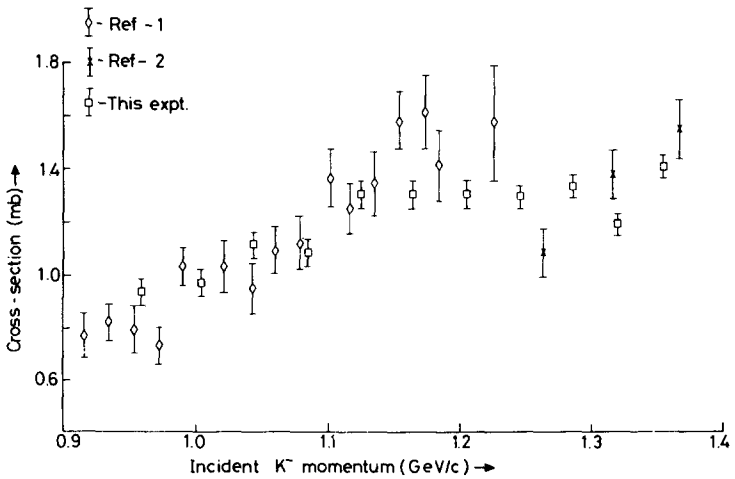

Fig. 1. Reaction (1) cross section as a function of incident momentum.

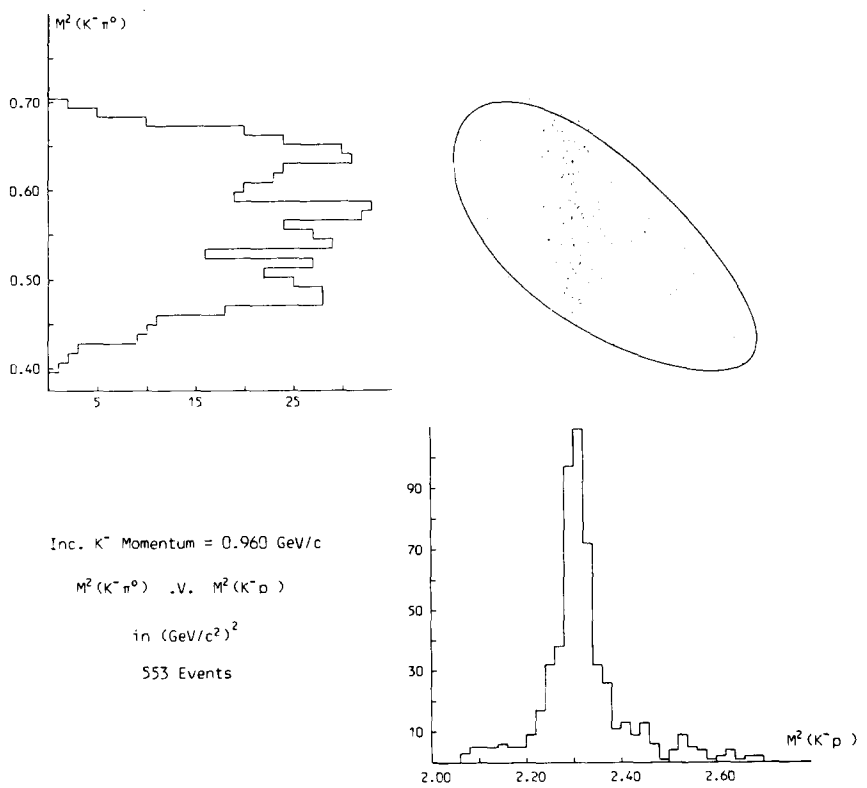

fig. 2(a).

ground to this distribution which has about 8000 events. The best fit has a χ^2 of 32 for 26 degrees of freedom and yields the following values for the resonance parameters:

$M = 1519.7 \pm 0.3$ MeV ,

$\Gamma = 16.3 \pm 0.5$ MeV .

The experimental resolution of 1 MeV for the Kp invariant mass has been included. The values obtained are in excellent agreement with those obtained in formation experiments [6] and the average values ($M = 1519 \pm 0.3$, $\Gamma = 15.1 \pm 0.5$) in ref. [7]. The 8000 events represent the largest sample of events from a production experiment used in the determination of these parameters. The background under the $\Lambda(1520)$ varies from a few per cent at the lowest momentum to around 30% at the highest.

The $K\pi$ mass-squared distribution in the region of the $K^*(890)$ ($0.675 \leqslant M^2_{K\pi} \leqslant 0.925$ GeV^2) has also been fitted to determine the parameters for this resonance. The results are presented elsewhere [8].

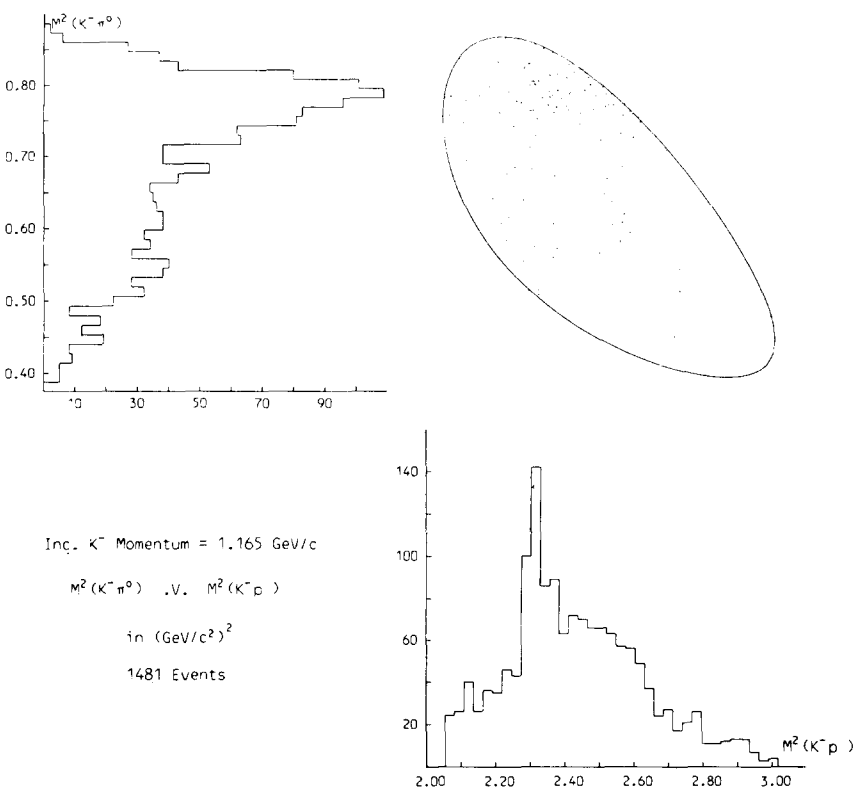

fig. 2(b).

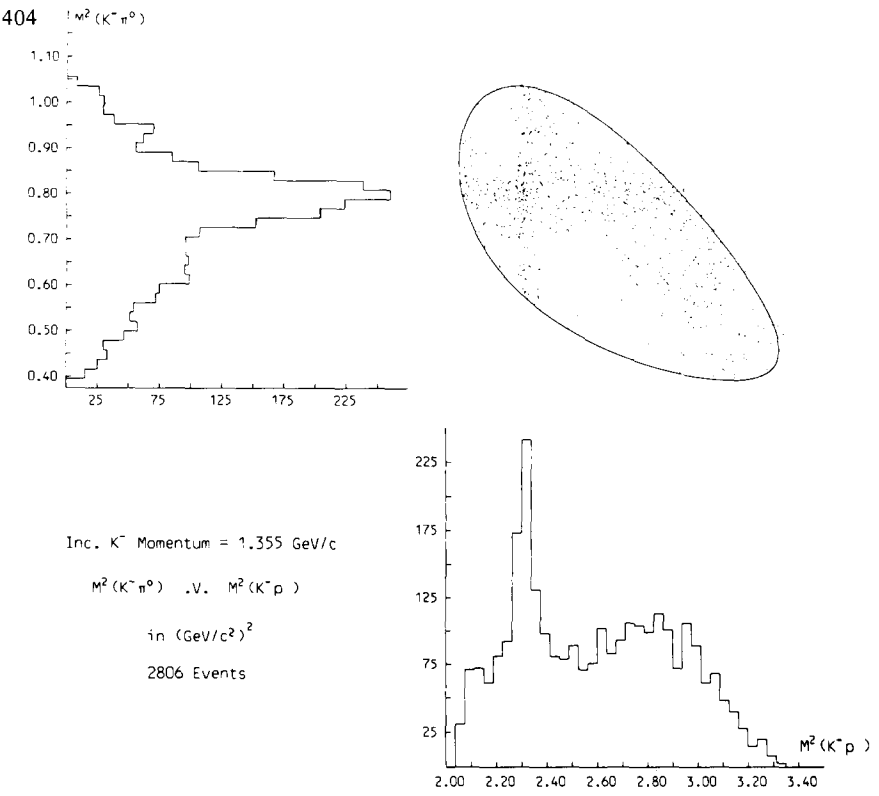

fig. 2(c).

Fig. 2. Dalitz plots (M^2(Kπ) *versus* M^2(Kp)) and projections at 0.960, 1.165 and 1.355 GeV/c K^- incident momenta.

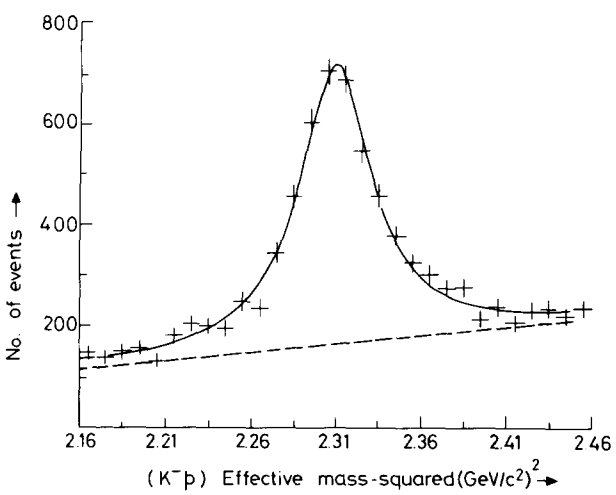

Fig. 3. M^2(Kp) distribution in the region of the Λ(1520). The curve is the result of the fit described in the text; the dashed line indicates the background under the resonance.

The $\Delta^+(1233)$ is almost as broad as the available phase space at any given incident energy in this region. It is therefore not possible to determine meaningful values for its mass and width from the present data. For the 4-variable fits to the 3-body final state, described in sect. 3, we have used the masses and widths given in ref. [7] for the Δ, $\Lambda(1690)$ and $\Sigma(1775)$ which have small contributions.

3. Extraction of the $\pi^0\Lambda(1520)$ channel

In order to correct for the appreciable background under each contributing quasi two-body process we have developed a new method [9] which uses all four relevant independent variables describing the three-particle final state from an unpolarised target. The coefficients of the Legendre polynomial expansions of the differential cross section and density matrix elements for all quasi two-body processes included are extracted simultaneously. Interference effects between contributing processes have been neglected. We did not find it possible to parametrise the interference terms in a model-independent manner and still retain the directness of the method. The fact that the data are reasonably well fitted at all energies with an incoherent production model suggests that interference effects are small.

The probability distribution W for reaction (2) is given by:

$$W(\cos\theta^*, \theta, \phi, M^2) = \frac{3}{4\pi} B(M^2) \frac{1}{\sigma} \frac{\mathrm{d}\sigma}{\mathrm{d}\cos\theta^*}$$
$$\times \left[\tfrac{1}{2}\left(\tfrac{1}{3} + \cos^2\theta\right) + 2\left(\tfrac{1}{3} - \cos^2\theta\right)\rho_{33}(\cos\theta^*)\right.$$
$$\left. - 2\sqrt{\tfrac{1}{3}} \sin 2\theta \cos\phi \,\mathrm{Re}\,\rho_{31}(\cos\theta^*) - 2\sqrt{\tfrac{1}{3}} \sin^2\theta \cos 2\phi \,\mathrm{Re}\,\rho_{3-1}(\cos\theta^*)\right], \tag{5}$$

where θ^* is the c.m. production angle of the π^0, θ and ϕ are the decay angles in the helicity frame of the $\Lambda(1520)$, M^2 is the invariant K^-p mass-squared, $B(M^2)$ is the relativistic Breit-Wigner form (normalised to 1.0 over the available phase space) with energy-independent width for the $\Lambda(1520)$ and the expression in the square brackets describes the $\Lambda(1520)$ decay distribution in terms of the density matrix elements ρ_{33}, $\mathrm{Re}\,\rho_{31}$ and $\mathrm{Re}\,\rho_{3-1}$, which are themselves functions of the production angle.

Following the formalism set out by Deen [10] the differential cross section and the density matrix elements are expanded in Legendre polynomial series:

$$\frac{\mathrm{d}\sigma}{\mathrm{d}\cos\theta^*} = 2\pi\lambda\!\!\!^{-2} \sum_l A_l P_l^0(\cos\theta^*),$$

$$\rho_{33} \frac{\mathrm{d}\sigma}{\mathrm{d}\cos\theta^*} = 2\pi\lambda\!\!\!^{-2} \sum_l B_l P_l^0(\cos\theta^*),$$

Table 2
Values of experimental coefficients A_0, A_l/A_0, B_l/A_0, C_l/A_0 and D_l/A_0 tabulated for the 11 incident beam momenta
Table 2 (a)

Momentum (GeV/c)		$A_0 \times 10^3$	A_1/A_0	A_2/A_0	A_3/A_0	A_4/A_0	A_5/A_0	A_6/A_0	A_7/A_0
0.960		34.479	−0.508	0.528	0.042	0.248	0.190	0.008	−0.068
	+/−	2.011	0.128	0.168	0.201	0.235	0.254	0.270	0.297
1.005		30.941	−0.374	0.575	−0.271	0.164	−0.224	−0.422	−0.062
	+/−	2.025	0.145	0.184	0.208	0.240	0.258	0.277	0.296
1.045		24.800	0.066	0.467	0.437	0.188	−0.330	0.220	−0.051
	+/−	1.470	0.125	0.160	0.192	0.218	0.238	0.258	0.274
1.085		18.736	0.301	0.177	0.051	−0.045	−0.413	−0.051	−0.373
	+/−	1.335	0.136	0.174	0.203	0.223	0.247	0.266	0.295
1.125		19.149	0.471	0.592	0.320	−0.228	0.072	0.015	−0.400
	+/−	1.307	0.138	0.171	0.203	0.219	0.251	0.273	0.289
1.165		15.676	0.524	0.366	0.181	0.204	0.491	−0.284	−0.234
	+/−	1.084	0.131	0.172	0.194	0.221	0.246	0.264	0.278
1.205		13.251	0.601	0.682	0.063	−0.139	−0.769	0.219	−0.480
	+/−	0.992	0.153	0.189	0.233	0.269	0.300	0.331	0.364
1.245		12.305	0.643	0.775	−0.036	−0.144	−0.356	0.362	0.226
	+/−	0.860	0.144	0.174	0.219	0.233	0.264	0.293	0.308
1.285		16.770	0.422	0.809	0.305	0.404	−0.251	−0.478	−0.046
	+/−	1.069	0.133	0.172	0.191	0.216	0.242	0.272	0.295
1.320		14.782	0.018	1.171	−0.296	0.273	0.466	0.463	0.544
	+/−	1.110	0.167	0.210	0.255	0.288	0.318	0.344	0.371
1.355		18.292	0.126	0.832	−0.181	0.025	−0.350	0.054	0.433
	+/−	1.040	0.117	0.143	0.171	0.192	0.216	0.232	0.247

$$\text{Re}\,\rho_{31}\frac{d\sigma}{d\cos\theta^*} = 2\pi\lambda^2\sum_l C_l P_l^1(\cos\theta^*),$$

$$\text{Re}\,\rho_{3-1}\frac{d\sigma}{d\cos\theta^*} = 2\pi\lambda^2\sum_l D_l P_l^2(\cos\theta^*). \qquad (6)$$

Similar expressions are written for the other contributing quasi two-body processes. The highest order of expansion required was to $l = 7$.

The high Kp mass region is poorly fitted when only reactions (2), (3), (4) and Lorentz invariant phase space are included. The CHM [3] and CRSS [2,3] collaborations reported evidence for the production of the $\frac{5}{2}^+$ $\Lambda(1815)$. However, the high Kp effective mass region is not satisfactorily explained by the inclusion of this

Table 2(b)

Momentum (GeV/c)		B_0/A_0	B_1/A_0	B_2/A_0	B_3/A_0	B_4/A_0	B_5/A_0	B_6/A_0	B_7/A_0
0.960		0.273	−0.125	0.159	0.046	−0.092	−0.107	0.044	0.095
	+/−	0.038	0.080	0.103	0.121	0.143	0.156	0.164	0.185
1.005		0.170	0.009	0.143	0.057	0.052	−0.186	−0.105	0.152
	+/−	0.042	0.085	0.104	0.114	0.130	0.144	0.154	0.166
1.045		0.183	−0.087	0.031	0.029	−0.061	−0.100	0.124	0.035
	+/−	0.039	0.076	0.097	0.118	0.129	0.144	0.157	0.166
1.085		0.112	0.206	0.245	0.173	−0.007	−0.132	−0.382	−0.201
	+/−	0.044	0.083	0.107	0.121	0.133	0.146	0.158	0.187
1.125		0.144	0.218	0.309	0.154	−0.177	0.238	−0.076	−0.291
	+/−	0.044	0.088	0.107	0.123	0.129	0.148	0.162	0.174
1.165		0.127	0.024	0.198	0.123	−0.142	0.142	−0.208	−0.257
	+/−	0.042	0.079	0.101	0.114	0.131	0.142	0.150	0.159
1.205		0.347	0.113	0.209	−0.224	−0.382	−0.714	0.234	−0.273
	+/−	0.047	0.098	0.120	0.149	0.169	0.190	0.212	0.232
1.245		0.326	0.380	0.102	−0.092	−0.208	−0.020	−0.010	0.051
	+/−	0.044	0.092	0.110	0.137	0.143	0.168	0.187	0.195
1.285		0.218	0.334	0.143	0.380	−0.220	−0.274	0.005	−0.044
	+/−	0.039	0.081	0.104	0.114	0.123	0.137	0.153	0.171
1.320		0.187	0.069	0.179	0.256	−0.158	0.398	0.416	−0.009
	+/−	0.045	0.098	0.122	0.150	0.176	0.191	0.210	0.231
1.355		0.266	0.250	0.152	0.195	−0.112	−0.231	−0.064	0.277
	+/−	0.034	0.071	0.086	0.101	0.112	0.130	0.139	0.147

process. Greatly improved fits are obtained, especially at the higher incident momenta, by including the production of the $\frac{3}{2}^-$ $\Lambda(1690)$ and the $\frac{5}{2}^-$ $\Sigma(1775)$ instead.

The reliability of the $\pi^0\Lambda(1520)$ expansion coefficients extracted by this procedure was checked by comparison with results from two other procedures. One used the moments program developed by Litchfield [11] and the other used simple mass cuts with background subtraction. The results from the three methods were found to be consistent.

The relative cross sections determined for the various contributing processes at the relevant incident momenta are given in table 1. A complete set of coefficients for reaction (2) are given in table 2 and the more significant coefficients are shown in fig. 4. The coefficients for reaction (3), extracted simultaneously, will be published elsewhere [8].

Table 2(c)

Momentum (GeV/c)		C_0/A_0	C_1/A_0	C_2/A_0	C_3/A_0	C_4/A_0	C_5/A_0	C_6/A_0	C_7/A_0
0.960		0.0	−0.050	0.074	−0.004	0.046	0.027	−0.012	0.029
	+/−	0.0	0.048	0.037	0.032	0.028	0.027	0.025	0.023
1.005		0.0	−0.111	0.082	−0.072	0.047	0.024	0.028	0.021
	+/−	0.0	0.053	0.043	0.038	0.032	0.031	0.028	0.026
1.045		0.0	0.019	−0.023	−0.077	0.042	−0.007	−0.011	−0.002
	+/−	0.0	0.043	0.036	0.029	0.026	0.024	0.023	0.021
1.085		0.0	−0.041	−0.001	0.016	0.079	−0.020	−0.015	0.028
	+/−	0.0	0.056	0.046	0.037	0.032	0.029	0.027	0.025
1.125		0.0	−0.098	−0.050	0.032	0.044	0.008	−0.027	0.048
	+/−	0.0	0.049	0.039	0.031	0.030	0.026	0.025	0.023
1.165		0.0	−0.133	0.052	−0.020	0.007	−0.022	−0.049	0.065
	+/−	0.0	0.048	0.036	0.030	0.026	0.023	0.022	0.021
1.205		0.0	0.061	−0.051	−0.039	0.003	0.023	0.006	0.059
	+/−	0.0	0.049	0.042	0.036	0.030	0.027	0.025	0.022
1.245		0.0	−0.023	−0.017	0.016	0.100	0.015	0.021	0.009
	+/−	0.0	0.043	0.038	0.029	0.028	0.027	0.024	0.023
1.285		0.0	−0.133	−0.017	−0.059	0.045	0.006	−0.040	0.012
	+/−	0.0	0.044	0.037	0.034	0.029	0.027	0.024	0.022
1.320		0.0	−0.096	0.088	−0.038	0.120	−0.009	0.011	−0.014
	+/−	0.0	0.046	0.042	0.038	0.035	0.031	0.030	0.028
1.355		0.0	−0.094	−0.007	−0.082	0.098	0.030	0.052	0.016
	+/−	0.0	0.037	0.033	0.028	0.025	0.023	0.021	0.020

4. $\pi^0\Lambda(1520)$ partial-wave analysis

4.1. The data

The analysis of Litchfield et al. [3] included data from the CHM and CRSS collaborations. Both experiments cover essentially the same centre of mass energy region (1915–2170 MeV). Similarly, there is a substantial overlap between the data from the CH collaboration [1,12] and the data from this experiment. Following our previous practice [6] we have decided to use data from the more recent and higher statistics experiment in the regions of overlap. The data used in the present partial-wave analysis are listed in table 3.

The dominant features of the data are:

(i) the large bump in A_0 at ~1770 MeV and a smaller broader one at ~2000 MeV;

Table 2(d)

Momentum (GeV/c)		D_0/A_0	D_1/A_0	D_2/A_0	D_3/A_0	D_4/A_0	D_5/A_0	D_6/A_0	D_7/A_0
0.960		0.0	0.0	−0.040	0.016	−0.007	0.000	0.000	−0.003
	+/−	0.0	0.0	0.017	0.010	0.007	0.005	0.004	0.003
1.005		0.0	0.0	−0.036	−0.009	−0.011	0.000	0.003	−0.002
	+/−	0.0	0.0	0.019	0.011	0.008	0.006	0.004	0.004
1.045		0.0	0.0	−0.024	−0.003	−0.012	−0.004	0.008	−0.002
	+/−	0.0	0.0	0.017	0.009	0.006	0.005	0.004	0.003
1.085		0.0	0.0	−0.010	−0.010	−0.030	−0.008	−0.004	0.000
	+/−	0.0	0.0	0.019	0.011	0.007	0.005	0.004	0.003
1.125		0.0	0.0	−0.039	−0.011	0.002	0.016	0.005	0.001
	+/−	0.0	0.0	0.018	0.011	0.007	0.005	0.004	0.003
1.165		0.0	0.0	−0.003	0.000	0.002	0.014	0.015	0.003
	+/−	0.0	0.0	0.019	0.010	0.007	0.005	0.004	0.003
1.205		0.0	0.0	−0.050	−0.005	−0.008	−0.002	−0.006	−0.003
	+/−	0.0	0.0	0.017	0.011	0.008	0.006	0.004	0.004
1.245		0.0	0.0	−0.033	−0.018	−0.004	−0.004	0.010	−0.004
	+/−	0.0	0.0	0.016	0.011	0.007	0.005	0.004	0.003
1.285		0.0	0.0	−0.076	0.006	−0.007	0.003	0.001	0.005
	+/−	0.0	0.0	0.015	0.009	0.007	0.005	0.004	0.003
1.320		0.0	0.0	−0.009	0.005	0.001	−0.003	0.002	0.003
	+/−	0.0	0.0	0.017	0.011	0.008	0.006	0.005	0.004
1.355		0.0	0.0	−0.032	−0.044	−0.007	−0.008	−0.002	0.004
	+/−	0.0	0.0	0.014	0.009	0.006	0.004	0.003	0.003

(ii) the highly structured behaviour of A_1/A_0 which changes sign at 1815 MeV and again at 1960 MeV;

(iii) the coefficients A_3/A_0, B_0/A_0, B_1/A_0 and C_1/A_0 are also active in this energy region.

4.2. The parametrization

A partial-wave amplitude $T_{LL'2J}$, where L and L' are the incoming and outgoing orbital angular momenta and J is the total angular momentum, is parametrized as a sum of a background term and, if required, non-relativistic Breit-Wigner terms,

$$T = T_B + T_R \ , \tag{7}$$

where T_B is the background term and T_R is a sum of non-relativistic Breit-Wigner

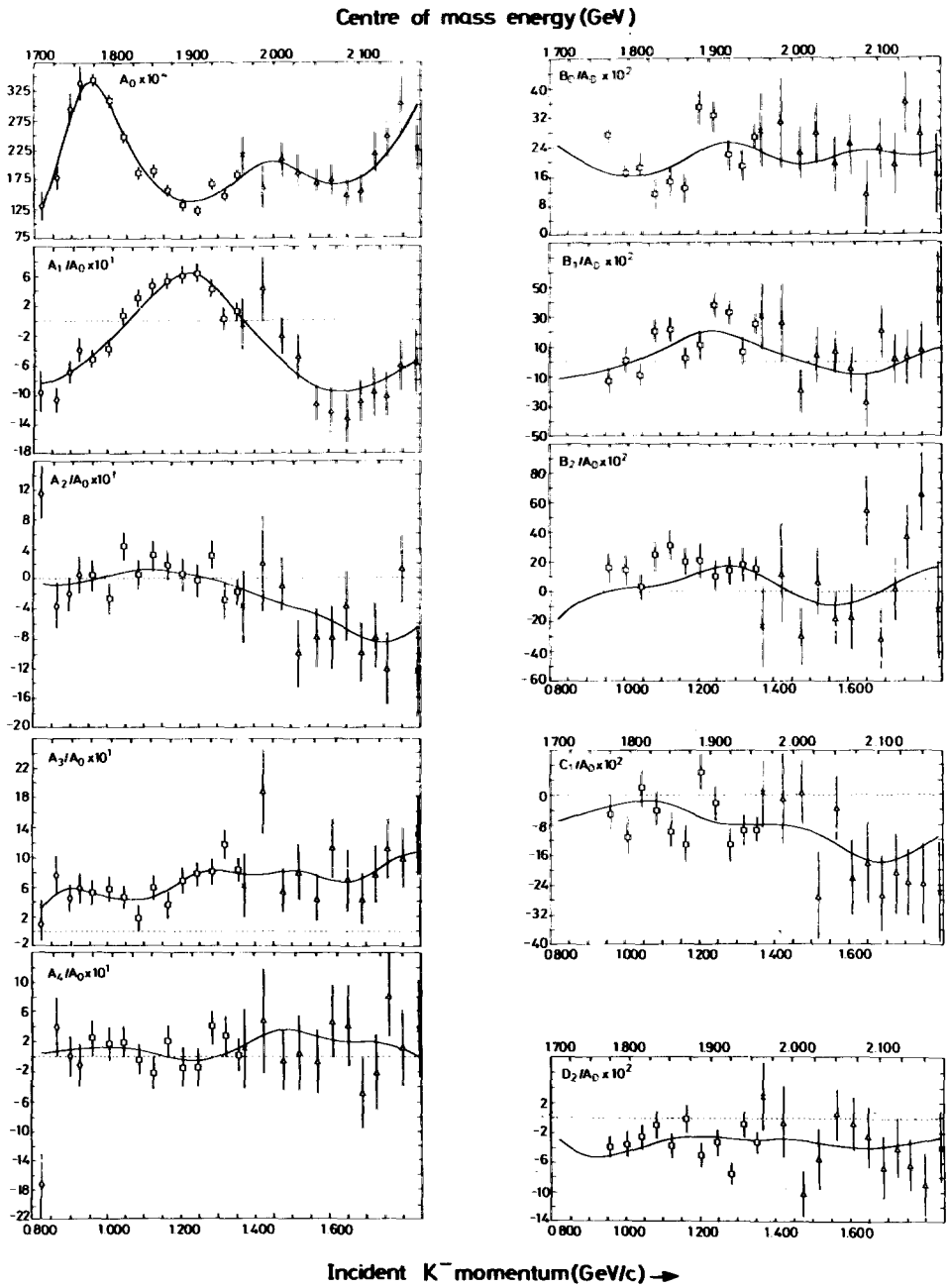

Fig. 4. A selection of Legendre polynomial expansion coefficients as a function of c.m. energy and incident beam momentum. The curve is the result of the partial-wave analysis (solution B). The data from present experiment, is shown by ϕ, the CH data by $\diamond$, the CRSS data by $\ast$ and the CHM data by $\dagger$.

Table 3
The data used in this analysis and the χ^2 contribution of each set given as χ^2/data point for solution B

Momentum range (GeV/c)		c.m. energy range (GeV/c)		Expt.	No. of momenta	Type of data	No. (N) of data points	χ^2/N
0.822	0.9255	1710	1759	CH [1]	4	A_0, A_l/A_0	28	1.50
0.960	1.355	1775	1957	This expt.	11	A_0, A_lA_0	88	1.06
						B_l/A_0	88	1.72
						C_l/A_0	77	1.46
						D_l/A_0	66	1.58
1.370	1.370	1964	1964	CRSS [2]	1	A_0, A_l/A_0	8	0.40
						B_l/A_0	8	0.50
						C_l/A_0	7	0.45
						D_l/A_0	7	0.80
1.424	1.798	1988	2150	CHM [3]	10	A_0, A_l/A_0	80	0.82
						B_l/A_0	80	1.02
						C_l/A_0	70	1.32
						D_l/A_0	60	1.26
1.841	1.841	2168	2168	CRSS [2]	1	A_0, A_l/A_0	8	0.71
						B_l/A_0	8	1.15
						C_l/A_0	7	0.62
						D_l/A_0	6	0.59

resonances of the form:

$$\frac{t}{\epsilon - i} e^{i\phi} , \tag{8}$$

where t is the resonance amplitude and $\epsilon = (2/\Gamma(E))\,(E_R - E)$. The energy dependent width Γ is of the form

$$\Gamma(E) = \Gamma(E_R)\frac{k v_l(kr)}{k_R v_l(k_R r)} , \tag{9}$$

where v_l is the Blatt and Weisskopf angular momentum barrier [13] for the incoming orbital angular momentum l. The radius of interaction, r, is taken to be 1 fm. In these formulae E is the centre of mass energy and E_R and k_R are the values of E and k at the resonance energy, and

$$t = \sqrt{XX'} = \sqrt{\frac{\Gamma_e\Gamma_i}{\Gamma^2}} ,$$

Γ_e and Γ_i being the partial widths of the elastic and the $\pi^0\Lambda(1520)$ channel. The elastic partial width Γ_e has the same energy dependence as the total width. For Γ_i, k and k_R in the formula correspond to the centre of mass momenta of the outgoing particles and l refers to the outgoing orbital angular momentum. It should be pointed

out that the specific form assumed for the energy dependence of the width does not affect the results significantly.

The background term has the form:

$$T_B = \sqrt{B_l B_{l'}} R(E)\, e^{i\theta(E)}\,, \tag{10}$$

where

$$R(E) = \sum_{m=0}^{M} a_m P_m(E')\,, \qquad \theta(E) = \sum_{n=0}^{N} b_n P_n(E')\,,$$

$$E' = \frac{2E - E_{max} - E_{min}}{E_{max} - E_{min}}\,,$$

such that E' equals +1 and −1 at energies E_{max} and E_{min} just above the upper end and below the lower end of the energy range fitted, and P_L are Legendre polynomials. The background parameters a_m and b_n are determined by fitting. The angular momentum barrier factor B_l has the form

$$B_l = \frac{k}{k_{max}} \frac{E_{max}}{E} \frac{v_l(kr)}{v_l(k_{max}r)}\,. \tag{11}$$

The various expansion coefficients of eq. (6) may be related to the partial-wave amplitudes by:

$$\eta_l = \sum_{L_1 L_1' J_1} \sum_{L_2 L_2' J_2} x_{L_1 L_1' J_1}^{L_2 L_2' J_2} \,\mathrm{Re}(T_{L_1 L_1' J_1} T^*_{L_2 L_2' J_2})\,, \tag{12}$$

where η_l is any of the coefficients $A_l - D_l$, and the x are the quasi two-body equivalents of the Tripp coefficients [14].

4.3. Development of the partial-wave solution

Over the energy range 1710–2170 MeV there are four established $I = 1$ states, the D5 Σ(1775), the F7 Σ(2040), the F5 Σ(1920) and the D3 Σ(1670), of which the first two are dominant. In addition to these states our partial-wave analyses of two-body final states [6] indicate the presence of five more 'probable' or 'possible' states, the S1 Σ(1770), S1 Σ(1955), P1 Σ(1676), P1 Σ(1732) and the D3 Σ(1940).

An initial partial-wave solution was developed with the four established resonances and simple two parameter background amplitudes ($N = M = 0$ in the equation (10)). The masses and widths of all resonances were fixed to values given in reference [6]. The overall phase was chosen such that the P-wave decay amplitude at resonance of the D5 Σ(1775) was purely imaginary. The phases of all other resonant amplitudes were allowed to vary in the initial stages of the fitting. Where a particular phase stayed close to 0 or π it was then fixed to this value. This solu-

tion, A, fits the data with a χ^2 of 943 for 655 degrees of freedom.

Into this base solution the 'probable' and 'possible' resonances were successively introduced. Individually none of these lead to any significant improvement in the fit, however where a resonance acquired an amplitude ($\sqrt{XX^\dagger}$) greater than 0.015 it was retained. Collectively the improvement is marginal (the χ^2 drops by only 19 for an additional 3 resonant amplitudes). The decay amplitudes of established resonances were fixed to 0 if smaller than 0.015. The D- and G-wave decays of the F5 $\Sigma(1920)$ were both in this class, and of the D3 $\Sigma(1690)$ only the P-wave decay was retained. The P-wave decay of the D5 $\Sigma(1775)$ and the D- and G-wave decays of the F7 $\Sigma(2040)$ were found to dominate.

To search for other waves that may be more active than allowed for in this solution, the number of background parameters was increased from two to four ($N = M = 1$) for each wave in turn. Significant improvements in χ^2 were obtained only for the S1, P3, F7 and G7 waves. However none of these background amplitudes showed significant anti-clockwise loops in the Argand diagrams. The solution, B, with 4-parameter backgrounds in these waves gives a χ^2 of 863 for 639 degrees of freedom.

Even in solution, B, the c.m. energy region 1830–1950 MeV is comparatively poorly fitted. Efforts to improve the fit to the data in this region with one or more resonances having widths greater than 20 MeV were unsuccessful. The fit to this region can be improved if this limit is relaxed. For example an improvement of 25 in the χ^2 is obtained with a D5 resonance at ~1875 MeV with a width of ~13 MeV. However, such narrow structures essentially come from data at a single energy, and the present statistics do not allow the necessary finer binning in energy to establish

Table 4
Resonant amplitudes for decays to $\pi\Lambda(1520)$

Resonance	Status [a]	Elasticity [a] (x)	Outgoing wave	$\pi\Lambda(1520)$ amplitude $\sqrt{XX^\dagger}$	$\pi\Lambda(1520)$ branching fraction
S1(1770)	probable	0.15 ± 0.03	P	±0.032 ± 0.021	0.007 ± 0.009
S1(1955)	probable	0.44 ± 0.05	P	−0.081 ± 0.021	0.015 ± 0.008
D3(1670)	established	0.08 ± 0.03	P	±0.081 ± 0.016	0.082 ± 0.045
			F	<0.03	
D3(1920)	possible	<0.04	P	<0.03	
			F	±0.062 ± 0.021	>0.096
D5(1775)	established	0.41 ± 0.03	P	0.303 ± 0.010	0.224 ± 0.022
			F	0.037 ± 0.014	0.003 ± 0.002
F7(2040)	established	0.24 ± 0.02	D	−0.114 ± 0.010	0.054 ± 0.010
			G	−0.146 ± 0.010	0.089 ± 0.014

[a] From ref. [6]. The sign of a resonance amplitude is indicated by ± when the presence of a large and active background amplitude causes the anticlockwise loop to point sideways at the resonance mass (convention: meson first, baryon second).

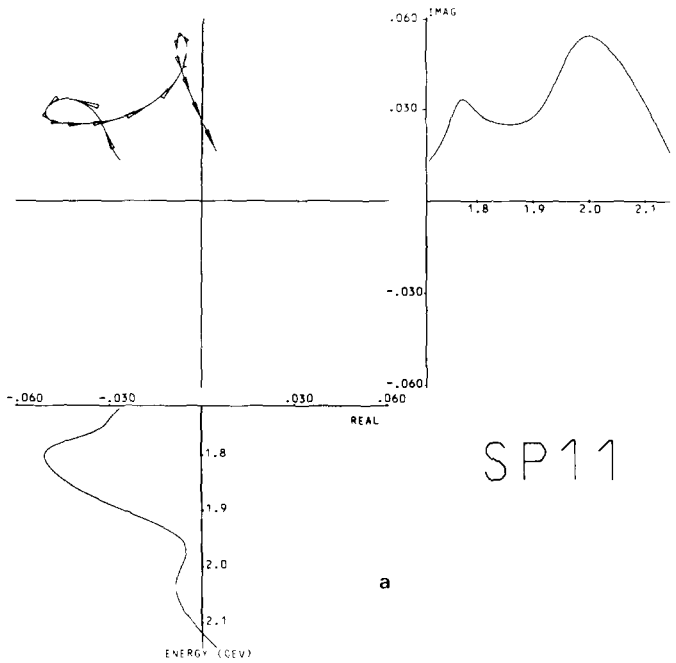
IMAG
.060
.030
-.030
-.060
1.8
1.9
2.0
2.1
-.060
-.030
.030
.060
REAL
ENERGY (GEV)
SP11
a

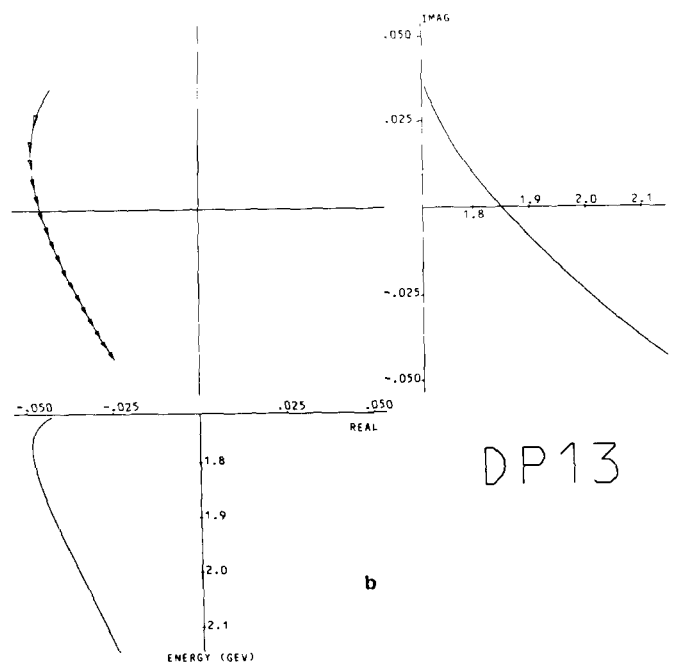
IMAG
.050
.025
-.025
-.050
1.8
1.9
2.0
2.1
-.050
-.025
.025
.050
REAL
ENERGY (GEV)
DP13
b

Fig. 5.

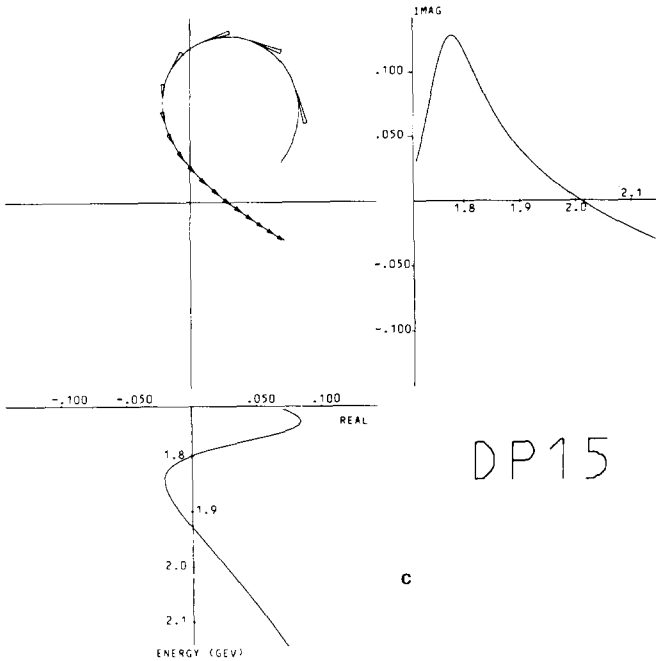

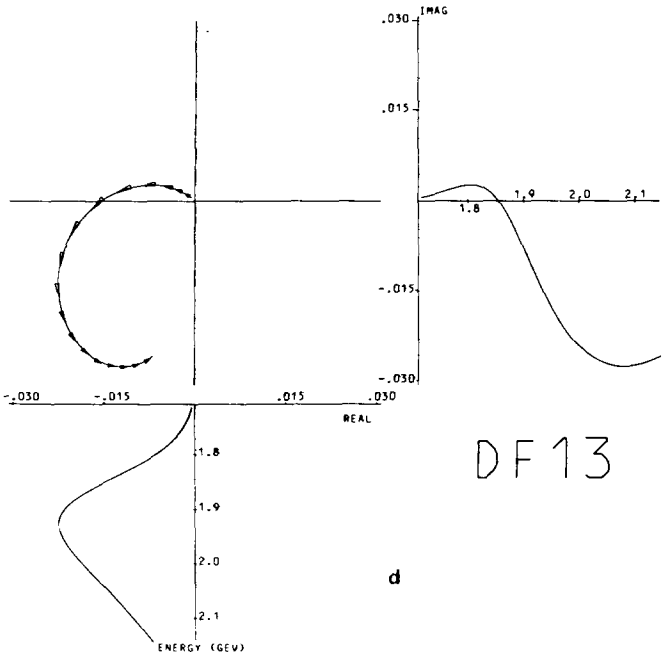

Fig. 5 (continued).

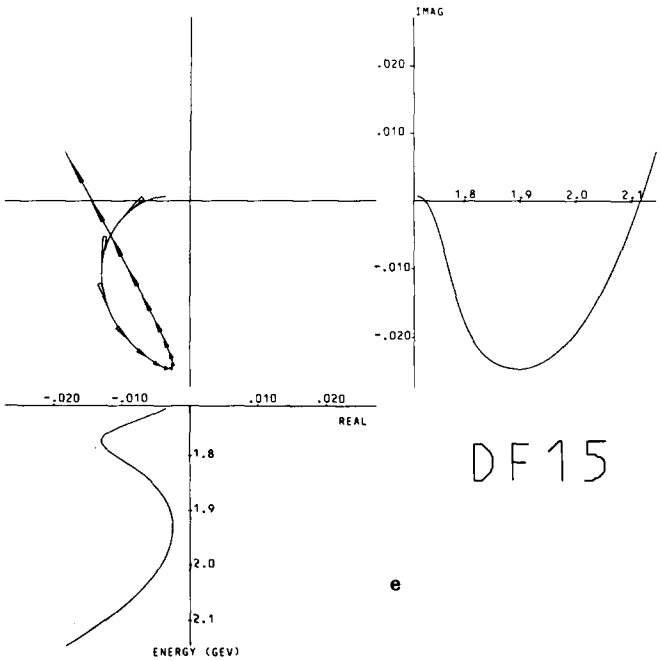

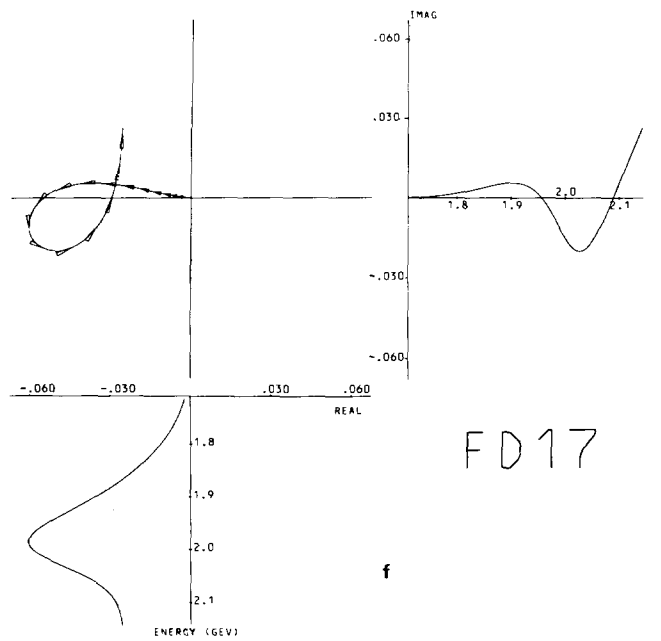

Fig. 5 (continued).

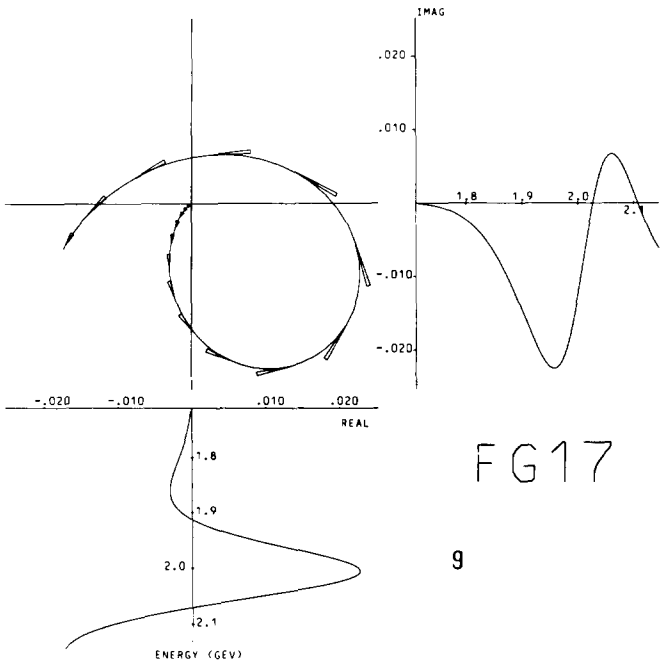

Fig. 5. Some Argand diagrams corresponding to solution B.

such structures reliably. In addition the mass and width of each resonance were allowed to vary, but no significant change was observed. The preferred solution therefore, for the $\pi\Lambda(1520)$ channel over the centre of mass energy range 1710–2170 MeV, remains solution B.

The quality of the fit to each data set is indicated in table 3 and shown in fig. 4 for the more significant coefficients. The resonant amplitudes for the complete $\pi\Lambda(1520)$ channel, using a branching fraction for $\Lambda(1520) \to K^-p$ of 0.23 [7], are given in table 4. The partial-wave amplitudes are presented at every 10 MeV centre of mass interval in table 5 and the Argand diagrams for the active partial waves shown in fig. 5. It should be noted that all amplitudes were obtained following the convention: meson first, baryon second.

5. Conclusions

Over the centre of mass energy region 1775 to 1960 MeV the $K^-p\pi^0$ final state is well explained by incoherent quasi two-body processes with a small amount of non-interfering three particle Lorentz invariant phase space, a conclusion also reached in the earlier experiments [1–3,12] below and above this energy region.

Table 5
$K^-p \to \pi^0\Lambda(1520)$ partial-wave amplitudes, given as real and imaginary parts for $\Lambda(1520)$ decaying to K^-p, at every 10 MeV c.m. energy interval

ECM	SP1	PD1	PS3	PD3	DP3	DF3	DP5	DF5	FD5	FG5	FD7	FG7	GF7	GH7	GF9
1.71	-0.26 0.12	-0.01 -0.02	-0.38 -0.15	0.02 0.02	-0.41 0.38	-0.00 0.00	0.64 0.24	-0.03 0.01	-0.00 -0.00	0.00 -0.00	-0.02 0.00	-0.00 -0.00	0.00 -0.00	0.00 -0.00	0.00 0.00
1.72	-0.28 0.14	-0.01 -0.02	-0.40 -0.16	0.03 0.02	-0.44 0.33	-0.01 0.01	0.75 0.38	-0.04 0.01	-0.00 -0.01	0.00 -0.00	-0.02 0.00	-0.00 -0.00	0.00 -0.00	0.00 -0.00	0.00 0.00
1.73	-0.29 0.17	-0.02 -0.02	-0.42 -0.16	0.04 0.02	-0.46 0.29	-0.01 0.01	0.82 0.56	-0.06 0.00	-0.00 -0.01	0.00 -0.00	-0.03 0.00	-0.00 -0.00	0.00 -0.00	0.00 -0.00	0.00 0.00
1.74	-0.31 0.21	-0.02 -0.03	-0.43 -0.16	0.05 0.01	-0.47 0.26	-0.01 0.01	0.84 0.77	-0.09 -0.01	-0.00 -0.01	0.00 -0.00	-0.04 0.00	-0.00 -0.00	0.00 -0.01	0.00 -0.00	0.00 0.00
1.75	-0.32 0.25	-0.03 -0.03	-0.45 -0.16	0.06 0.00	-0.48 0.22	-0.02 0.01	0.78 0.98	-0.11 -0.03	-0.01 -0.01	0.00 -0.00	-0.05 0.00	-0.01 -0.01	0.00 -0.01	0.00 -0.00	0.00 0.00
1.76	-0.36 0.30	-0.03 -0.04	-0.46 -0.16	0.07 -0.01	-0.48 0.19	-0.02 0.02	0.65 1.15	-0.12 -0.06	-0.01 -0.02	0.00 -0.00	-0.06 0.01	-0.01 -0.01	0.00 -0.01	0.00 -0.00	0.00 0.00
1.77	-0.41 0.33	-0.03 -0.05	-0.47 -0.16	0.08 -0.02	-0.48 0.17	-0.03 0.02	0.47 1.26	-0.13 -0.09	-0.01 -0.02	0.00 -0.00	-0.07 0.01	-0.01 -0.01	0.00 -0.02	0.00 -0.00	0.00 0.00
1.78	-0.47 0.33	-0.04 -0.05	-0.48 -0.16	0.08 -0.04	-0.48 0.14	-0.04 0.02	0.28 1.29	-0.13 -0.13	-0.01 -0.02	0.00 -0.00	-0.08 0.01	-0.01 -0.01	0.00 -0.02	0.00 -0.00	0.00 0.00
1.79	-0.50 0.31	-0.04 -0.06	-0.49 -0.16	0.08 -0.05	-0.48 0.12	-0.05 0.03	0.12 1.26	-0.12 -0.15	-0.01 -0.03	0.00 -0.00	-0.10 0.01	-0.01 -0.02	-0.00 -0.03	0.00 -0.00	0.00 0.00
1.80	-0.51 0.29	-0.05 -0.07	-0.50 -0.15	0.08 -0.07	-0.48 0.10	-0.06 0.03	-0.01 1.19	-0.11 -0.18	-0.01 -0.03	0.00 -0.00	-0.11 0.02	-0.02 -0.02	-0.00 -0.03	0.00 -0.01	0.00 0.00
1.81	-0.51 0.28	-0.05 -0.07	-0.51 -0.15	0.07 -0.09	-0.48 0.08	-0.08 0.03	-0.11 1.10	-0.10 -0.20	-0.02 -0.03	0.00 -0.00	-0.13 0.02	-0.02 -0.03	-0.01 -0.04	0.01 -0.01	0.00 0.00
1.82	-0.50 0.27	-0.06 -0.08	-0.52 -0.15	0.06 -0.11	-0.47 0.06	-0.09 0.02	-0.16 1.00	-0.09 -0.21	-0.02 -0.04	0.00 -0.00	-0.15 0.02	-0.02 -0.04	-0.02 -0.04	0.01 -0.01	0.00 0.00
1.83	-0.48 0.26	-0.07 -0.09	-0.52 -0.15	0.04 -0.13	-0.47 0.04	-0.11 0.02	-0.20 0.90	-0.07 -0.22	-0.02 -0.04	0.00 -0.00	-0.17 0.03	-0.03 -0.05	-0.02 -0.05	0.01 -0.01	0.00 0.00
1.84	-0.46 0.25	-0.07 -0.10	-0.53 -0.14	0.02 -0.14	-0.46 0.02	-0.13 0.01	-0.21 0.81	-0.06 -0.23	-0.02 -0.05	0.00 -0.00	-0.19 0.03	-0.03 -0.06	-0.03 -0.05	0.01 -0.01	0.00 0.00
1.85	-0.44 0.25	-0.08 -0.10	-0.54 -0.14	-0.00 -0.15	-0.46 0.00	-0.15 0.01	-0.21 0.73	-0.06 -0.24	-0.03 -0.05	0.00 -0.00	-0.21 0.04	-0.03 -0.07	-0.04 -0.05	0.02 -0.01	0.01 0.00
1.86	-0.41 0.25	-0.08 -0.11	-0.54 -0.13	-0.03 -0.16	-0.45 -0.02	-0.16 -0.01	-0.20 0.65	-0.05 -0.24	-0.03 -0.06	0.00 -0.01	-0.23 0.04	-0.03 -0.08	-0.05 -0.05	0.02 -0.01	0.01 0.00
1.87	-0.38 0.25	-0.09 -0.12	-0.55 -0.13	-0.06 -0.16	-0.44 -0.03	-0.18 -0.02	-0.18 0.58	-0.04 -0.24	-0.03 -0.07	0.00 -0.01	-0.26 0.05	-0.03 -0.09	-0.07 -0.05	0.02 -0.01	0.01 0.00
1.88	-0.34 0.26	-0.10 -0.13	-0.55 -0.12	-0.09 -0.16	-0.44 -0.05	-0.20 -0.04	-0.16 0.52	-0.04 -0.24	-0.03 -0.07	0.00 -0.01	-0.29 0.05	-0.03 -0.11	-0.08 -0.05	0.03 -0.01	0.01 0.00
1.89	-0.30 0.26	-0.10 -0.14	-0.55 -0.12	-0.12 -0.15	-0.43 -0.07	-0.21 -0.06	-0.13 0.46	-0.03 -0.25	-0.04 -0.08	0.00 -0.01	-0.32 0.05	-0.02 -0.13	-0.09 -0.04	0.03 -0.01	0.01 0.00
1.90	-0.26 0.27	-0.11 -0.15	-0.55 -0.12	-0.14 -0.13	-0.43 -0.09	-0.22 -0.08	-0.10 0.41	-0.03 -0.25	-0.04 -0.09	0.01 -0.01	-0.35 0.06	-0.02 -0.15	-0.11 -0.04	0.03 -0.01	0.01 0.00
1.91	-0.21 0.29	-0.12 -0.16	-0.56 -0.11	-0.17 -0.11	-0.42 -0.10	-0.22 -0.10	-0.06 0.36	-0.03 -0.25	-0.05 -0.10	0.01 -0.01	-0.39 0.05	-0.00 -0.16	-0.12 -0.03	0.04 -0.01	0.01 0.00
1.92	-0.17 0.32	-0.13 -0.17	-0.56 -0.10	-0.19 -0.08	-0.41 -0.12	-0.23 -0.12	-0.03 0.31	-0.03 -0.24	-0.05 -0.10	0.01 -0.01	-0.42 0.05	0.01 -0.18	-0.13 -0.01	0.04 -0.01	0.01 0.00
1.93	-0.13 0.35	-0.13 -0.18	-0.56 -0.10	-0.21 -0.05	-0.40 -0.13	-0.23 -0.14	0.00 0.27	-0.03 -0.24	-0.05 -0.11	0.01 -0.01	-0.46 0.04	0.03 -0.20	-0.15 0.00	0.05 -0.01	0.02 0.00
1.94	-0.10 0.39	-0.14 -0.19	-0.56 -0.09	-0.22 -0.02	-0.40 -0.15	-0.22 -0.16	0.04 0.23	-0.03 -0.24	-0.06 -0.12	0.01 -0.02	-0.49 0.03	0.05 -0.21	-0.15 0.02	0.06 -0.01	0.02 0.00
1.95	-0.07 0.43	-0.15 -0.20	-0.56 -0.09	-0.22 0.02	-0.39 -0.17	-0.22 -0.18	0.08 0.19	-0.03 -0.23	-0.06 -0.13	0.01 -0.02	-0.53 0.02	0.08 -0.22	-0.16 0.04	0.06 -0.01	0.02 0.00
1.96	-0.06 0.46	-0.15 -0.21	-0.56 -0.08	-0.22 0.06	-0.38 -0.18	-0.22 -0.19	0.11 0.16	-0.03 -0.23	-0.07 -0.14	0.01 -0.02	-0.56 -0.01	0.11 -0.22	-0.16 0.06	0.07 -0.01	0.02 0.00
1.97	-0.05 0.50	-0.16 -0.22	-0.56 -0.08	-0.21 0.09	-0.38 -0.20	-0.21 -0.21	0.15 0.12	-0.03 -0.22	-0.07 -0.15	0.01 -0.02	-0.59 -0.04	0.15 -0.22	-0.16 0.08	0.07 -0.01	0.03 0.01
1.98	-0.06 0.52	-0.17 -0.23	-0.55 -0.07	-0.20 0.13	-0.37 -0.21	-0.20 -0.22	0.18 0.09	-0.03 -0.21	-0.08 -0.16	0.01 -0.03	-0.60 -0.07	0.18 -0.20	-0.16 0.10	0.08 -0.00	0.03 0.01
1.99	-0.06 0.54	-0.18 -0.24	-0.55 -0.07	-0.18 0.16	-0.36 -0.23	-0.20 -0.23	0.22 0.06	-0.04 -0.20	-0.08 -0.17	0.02 -0.03	-0.61 -0.11	0.21 -0.17	-0.15 0.12	0.08 0.00	0.03 0.01
2.00	-0.07 0.55	-0.19 -0.25	-0.55 -0.06	-0.15 0.19	-0.35 -0.24	-0.19 -0.24	0.25 0.03	-0.04 -0.19	-0.09 -0.18	0.02 -0.03	-0.60 -0.15	0.23 -0.12	-0.14 0.14	0.08 0.00	0.03 0.01
2.01	-0.08 0.54	-0.19 -0.26	-0.55 -0.06	-0.12 0.21	-0.35 -0.25	-0.18 -0.25	0.29 0.00	-0.05 -0.18	-0.09 -0.19	0.02 -0.04	-0.57 -0.18	0.23 -0.08	-0.13 0.16	0.08 0.01	0.04 0.01
2.02	-0.08 0.54	-0.20 -0.27	-0.54 -0.05	-0.08 0.23	-0.34 -0.27	-0.17 -0.26	0.32 -0.03	-0.05 -0.17	-0.10 -0.20	0.02 -0.04	-0.53 -0.20	0.21 -0.03	-0.11 0.17	0.09 0.01	0.04 0.01
2.03	-0.09 0.52	-0.21 -0.28	-0.54 -0.04	-0.04 0.24	-0.33 -0.28	-0.16 -0.26	0.36 -0.05	-0.06 -0.16	-0.10 -0.21	0.02 -0.05	-0.49 -0.20	0.18 0.01	-0.09 0.18	0.08 0.02	0.05 0.01
2.04	-0.09 0.50	-0.22 -0.29	-0.53 -0.04	-0.00 0.24	-0.32 -0.30	-0.15 -0.27	0.39 -0.08	-0.07 -0.14	-0.11 -0.23	0.03 -0.05	-0.45 -0.19	0.14 0.04	-0.07 0.18	0.08 0.02	0.05 0.01
2.05	-0.08 0.48	-0.22 -0.30	-0.53 -0.03	0.04 0.24	-0.32 -0.31	-0.15 -0.27	0.43 -0.10	-0.08 -0.13	-0.11 -0.24	0.03 -0.06	-0.40 -0.16	0.09 0.06	-0.04 0.18	0.08 0.02	0.05 0.01
2.06	-0.08 0.45	-0.23 -0.31	-0.52 -0.03	0.07 0.23	-0.31 -0.32	-0.14 -0.27	0.46 -0.12	-0.08 -0.11	-0.12 -0.25	0.03 -0.06	-0.37 -0.13	0.05 0.07	-0.02 0.17	0.07 0.02	0.06 0.01
2.07	-0.07 0.42	-0.24 -0.32	-0.52 -0.02	0.11 0.21	-0.30 -0.34	-0.13 -0.28	0.49 -0.15	-0.09 -0.09	-0.12 -0.26	0.04 -0.07	-0.34 -0.09	0.00 0.06	-0.00 0.16	0.06 0.02	0.06 0.01
2.08	-0.06 0.39	-0.25 -0.33	-0.51 -0.02	0.14 0.19	-0.29 -0.35	-0.12 -0.28	0.53 -0.17	-0.10 -0.08	-0.13 -0.27	0.04 -0.07	-0.31 -0.04	-0.04 0.05	0.01 0.14	0.05 0.02	0.07 0.01
2.09	-0.04 0.36	-0.25 -0.34	-0.51 -0.01	0.17 0.16	-0.29 -0.36	-0.11 -0.28	0.56 -0.19	-0.11 -0.06	-0.14 -0.29	0.04 -0.08	-0.29 0.01	-0.08 0.04	0.02 0.11	0.04 0.02	0.08 0.02
2.10	-0.03 0.33	-0.26 -0.35	-0.50 -0.01	0.19 0.13	-0.28 -0.38	-0.10 -0.27	0.59 -0.21	-0.13 -0.03	-0.14 -0.30	0.05 -0.09	-0.28 0.05	-0.11 0.02	0.02 0.08	0.03 0.01	0.08 0.02
2.11	-0.02 0.29	-0.27 -0.36	-0.49 -0.00	0.20 0.09	-0.27 -0.39	-0.10 -0.27	0.62 -0.23	-0.14 -0.01	-0.15 -0.31	0.05 -0.10	-0.27 0.10	-0.13 -0.00	0.02 0.04	0.01 0.00	0.09 0.02
2.12	0.00 0.26	-0.28 -0.37	-0.48 0.00	0.21 0.06	-0.26 -0.40	-0.09 -0.27	0.66 -0.25	-0.15 0.01	-0.15 -0.33	0.06 -0.10	-0.27 0.15	-0.15 -0.02	0.00 0.00	-0.01 -0.01	0.10 0.02
2.13	0.02 0.22	-0.28 -0.38	-0.48 0.01	0.21 0.02	-0.26 -0.42	-0.08 -0.27	0.69 -0.27	-0.16 0.03	-0.16 -0.34	0.06 -0.11	-0.26 0.20	-0.16 -0.04	-0.03 -0.04	-0.04 -0.03	0.10 0.02
2.14	0.04 0.18	-0.29 -0.39	-0.47 0.01	0.20 -0.01	-0.25 -0.43	-0.07 -0.26	0.72 -0.29	-0.18 0.06	-0.17 -0.35	0.06 -0.12	-0.26 0.24	-0.17 -0.06	-0.07 -0.08	-0.06 -0.05	0.11 0.02
2.15	0.05 0.14	-0.30 -0.40	-0.46 0.01	0.19 -0.04	-0.24 -0.44	-0.07 -0.26	0.75 -0.31	-0.19 0.09	-0.17 -0.37	0.07 -0.13	-0.26 0.29	-0.18 -0.07	-0.13 -0.11	-0.09 -0.08	0.12 0.02
2.16	0.07 0.10	-0.31 -0.41	-0.45 0.02	0.17 -0.07	-0.23 -0.45	-0.06 -0.25	0.78 -0.33	-0.21 0.11	-0.18 -0.38	0.07 -0.14	-0.25 0.33	-0.18 -0.07	-0.20 -0.13	-0.12 -0.12	0.13 0.03
2.17	0.09 0.06	-0.31 -0.42	-0.44 0.02	0.15 -0.09	-0.23 -0.46	-0.05 -0.24	0.81 -0.34	-0.22 0.14	-0.19 -0.39	0.08 -0.15	-0.25 0.38	-0.18 -0.07	-0.28 -0.15	-0.15 -0.16	0.13 0.03

A new determination of the mass and width of the $\Lambda(1520)$ has been made. Data from this and earlier experiments have been used to determine the partial wave amplitudes for the $\pi^0\Lambda(1520)$ channel. These, in general, give a good description of the data but structures are present which can only be explained by resonances too narrow to be reliably established.

From 1710–1850 MeV the channel is dominated by the P-wave decay of the D5 $\Sigma(1775)$. At higher energies the dominant feature is found to be the formation of the F7 $\Sigma(2040)$. In contrast to the results from the partial-wave analysis of Litchfield et al. [2], carried out over the narrower centre of mass energy region 1915–2170 MeV, we find the F7 resonance decaying almost equally to the D- and G-waves. Our use of the data from the more recent and higher statistics experiment and the different type of background parametrization used might explain this difference. Of the less well-established resonances the S1 $\Sigma(1770)$, the S1 $\Sigma(1955)$ and the D3 $\Sigma(1940)$ have appreciable couplings to this channel, although their status is not particularly enhanced. It is also found that the S1, P3, F7 and G7 waves have fairly large and active background amplitudes. It should be noted that, as in the $\bar{K}N$ two-body channels, there is no evidence for P3 Σ resonances.

All states considered in this analysis have been assigned to higher supermultiplets of SU(6). There have been several phenomenological investigations of their decays to the ground $[56, 0^+]$ supermultiplet. The present results permit extension of such investigations to decays to the $[70, 1^-]$ supermultiplet.

Three of us (RWMH, PN and RAS) are grateful to Science Research Council for financial support.

References

[1] D. Merrill, W. Barletta, B. Conforto, D. Harmsen, T. Laskinski, R. Levi-Setti, E. Burkhardt and H. Oberlach, Nucl. Phys. B60 (1973) 315.

[2] A. De Bellefon, A. Berthon, L.K. Rangan, J. Vrana, T.C. Bacon, A. Brandstetter, I. Butterworth, S.M. Deen, C.M. Fisher, P.J. Litchfield, R.J. Miller, J.R. Smith, G. Burgun, J. Meyer, E. Pauli, G. Poulard, B. Tallini, W. Wojcik, J. Zatz and R. Strub, Nuovo Cim. 7A (1972) 567;
A. Berthon, G. Tristram, J. Vrana, T.C. Bacon, A.A. Brandstetter, I. Butterworth, G.P. Gopal, P.S. Jones, P.J. Litchfield, M. Mandelkern, J. Meyer, G. Poulard, B. Tallini, W. Wojcik, J. Zatz and R. Strub, Nuovo Cim. 21A (1974) 146.

[3] P.J. Litchfield, R.J. Hemingway, P. Baillon, A. Putzer and M. Schleich, Nucl. Phys. B74 (1974) 39.

[4] RL-IC Collaboration, B. Conforto, G.P. Gopal, G.E. Kalmus, P.J. Litchfield, R.T. Ross, A.J. Van Horn, T.C. Bacon, I. Butterworth, E.F. Clayton and R.M. Waters, Nucl. Phys. B105 (1976) 189.

[5] J.D. Jackson, Nuovo Cim. 34 (1964) 1.

[6] RL-IC Collaboration, G.P. Gopal, R.T. Ross, A.J. Van Horn, A.C. McPherson, E.F. Clayton, T.C. Bacon and I. Butterworth, Nucl. Phys. B119 (1977) 362.

[7] Particle Data Group, Rev. Mod. Phys. 48 (1976) 1.

[8] RL-IC Collaboration, to be published.
[9] B. Franek, Rutherford Laboratory report RL 77 069/A, unpublished.
[10] S.M. Deen, Rutherford Laboratory preprint RPP/H/68, unpublished.
[11] P.J. Litchfield, Private communication.
[12] W.A. Barletta, Nucl. Phys. B40 (1972) 45.
[13] J.M. Blatt and V.F. Weisskopf, Theoretical nuclear physics (Wiley, New York, 1952) p. 361.
[14] B. Franek, Rutherford Laboratory Bubble Chamber Group Physics Note No. 110, unpublished.